ACS OMEGA

Open Access

http://pubs.acs.org/journal/acsodf

Article

Facile Synthesis of Bamboo Biochar for Efficient Adsorption of Quinolone Antibiotics: Effects and Mechanisms

Erming Ouyang, Ruiyue Zhang, WenJie Fu, Rui Zhao,* Hongwei Yang, Hanrui Xiang, and Wanyuan He

Cite This: *ACS Omega* 2024, 9, 48618−48628

Read Online

ACCESS | Metrics & More | Article Recommendations | Supporting Information

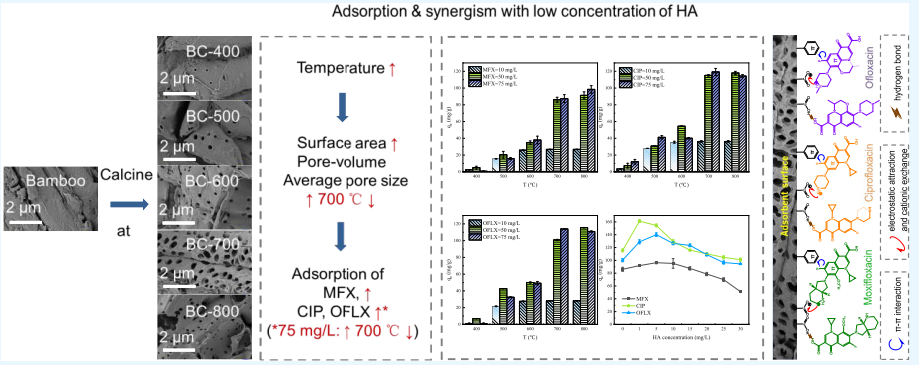

ABSTRACT: The harmful effects of quinolone antibiotics on ecology and human health have attracted widespread attention. In this study, bamboo biochar synthesized at different pyrolysis temperatures was used to remove quinolone antibiotics (moxifloxacin (MFX), ciprofloxacin (CIP), and ofloxacin (OFLX) as models). The pyrolysis temperature of 700 °C led to a high pore volume and average pore size of biochar. The biochar produced at 700 °C presented high adsorption properties for MFX, CIP, and OFLX. The maximum adsorption capacities for MFX, CIP, and OFLX were 135.56, 151.31, and 116.40 mg/g, respectively. The adsorption performance could be described by the Langmuir isotherm model and pseudo-second-order kinetic model. Biochar produced from waste bamboo could be applied as low-cost environmental adsorbents for quinolone antibiotics removal.

1. INTRODUCTION

Quinolone antibiotics, which were widely used to treat or prevent bacterial infections in humans and animals, could be released into the aquatic environment through incomplete metabolism of the body and discharge of livestock and medical wastewater.[1] Notably, quinolone antibiotics were persistent in the environment because of their low biodegradability and high polarity.[2] 30−90% of them were excreted in the form of original compounds and entered soil, sediments, and water.[3] It was reported that the concentration of quinolone antibiotics in surface water, groundwater, and wastewater ranged from ng/L to mg/L.[2] The highest concentration of quinolone antibiotics in wastewater from hospitals and antibiotic manufacturing units was 31 mg/L in Korea.[2,4] Moreover, the discharge of quinolone antibiotics posed a serious threat to public health and the environment by developing antibiotic-resistance bacteria or genes, thus reducing the therapeutic value of the drugs to pathogens and polluting drinking water.[5] Therefore, it is important and urgent to remove quinolone antibiotics from water.

Different remediation methods, including adsorption,[6,7] chemical oxidation,[8] and photocatalytic degradation,[9] had been developed to dislodge quinolone antibiotics. Of the available alternatives, adsorption was cost-effective and easy to operate in emergency pollution.[10,11] The quest for suitable and abundant precursors from nature had become a subject of considerable interest. Many natural and synthetic adsorbents, such as biochar,[12] graphene oxide,[13] and chitosan-based materials,[3] had been used to remove antibiotics from wastewater.[14] Among them, biochar has recently become an effective material for sewage treatment because of its high cost-effectiveness, easy access to biomass, slowing down climate change, and improving soil quality.[15]

At present, biochar prepared from rice straw,[16] wheat straw,[17] and bamboo[18] has been widely reported. China was the largest bamboo producer in the world.[18] A large amount of bamboo waste would be produced in the process of exploitation, processing, and utilization, and its utilization rate was only 35−40%.[19] Burying or burning bamboo waste would pollute the environment and waste bamboo resources.

Received: August 19, 2024
Revised: October 31, 2024
Accepted: November 12, 2024
Published: November 24, 2024

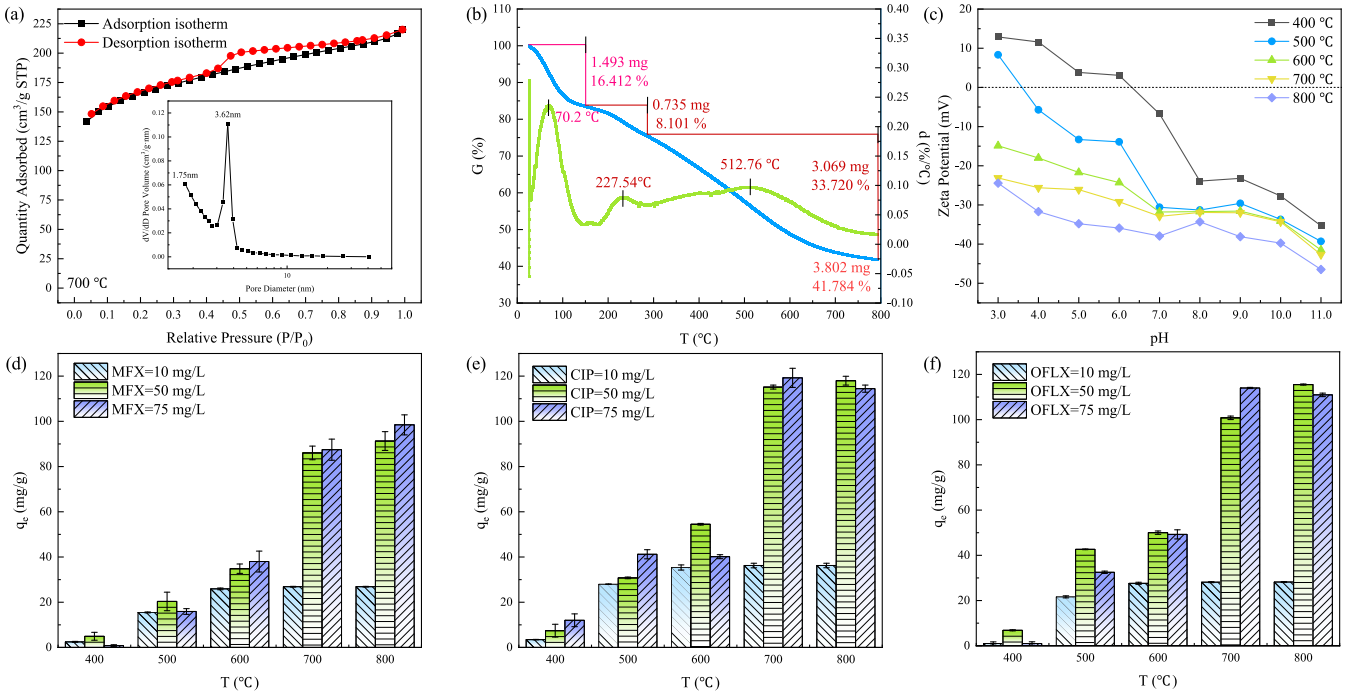

Figure 1. (a) N_2 adsorption−desorption isotherm and pore size distribution of BC-700; (b) TGA curves of raw bamboo; (c) ζ-potentials of bamboo biochar at different calcination temperatures at different pH values; and the (d−f) effect of calcination temperature on adsorption of BC-700 for MFX, CIP, and OFLX with different concentrations.

The high content of cellulose, hemicellulose, and lignin in bamboo gave them a larger surface area,[20] movable substances, and carbon content than biochar derived from animal waste and municipal solid waste.[21] Therefore, one of the best options for reusing waste biomass was to produce value-added biochar through the thermal process of pyrolysis so as to achieve the purpose of treating waste with waste.[22−25]

In this context, the study assessed the direct utilization of biochar derived from bamboo at various temperatures (i.e., 400, 500, 600, 700, and 800 °C) as the adsorbent for quinolone antibiotics (moxifloxacin (MFX), ciprofloxacin (CIP), and ofloxacin (OFLX) as models). Specifically, the adsorption performance was evaluated through isothermic, thermodynamic, and kinetic analyses, and the effects of solution pH, coexisting ions, and humic acid were considered. Furthermore, the possible mechanisms were elucidated using an analysis of characterization and experimental results.

2. EXPERIMENTAL SECTION

2.1. Materials. Moxifloxacin (MFX) hydrochloride, ciprofloxacin (CIP) hydrochloride monohydrate, and ofloxacin (OFLX) were supplied by Shanghai McLean Biochemical Technology Co., Ltd. The grade/purity of Moxifloxacin (MFX) hydrochloride, ciprofloxacin (CIP) hydrochloride monohydrate, and ofloxacin (OFLX) was 98%. All reagents were used directly without any further purification. Ultrapure water was used to prepare the aqueous solution.

2.2. Preparation of Adsorbent. The powder of bamboo was washed with pure water and dried at 80 °C for 24 h. Three grams of dried bamboo was put into a crucible with a cover and calcined in a muffle furnace (400, 500, 600, 700, and 800 °C, 2 h) at a heating rate of 7.8 °C/min. After cooling to room temperature, it was soaked repeatedly with pure water, washed until the pH of the supernatant was 7.0 ± 0.2, dried at 105 °C for 8 h, cooled to room temperature, packed in a sealed bag, and put into a dryer for later use.

2.3. Adsorption Experiment. In order to evaluate the adsorption effect of bamboo biochar synthesized at different pyrolysis temperatures on MFX, CIP, and OFLX in an aqueous solution, the adsorption experiments were carried out in brown bottles by shaking in 20 mL of MFX, CIP, and OFLX solution at 180 rpm for 12 h. The adsorption capacity was calculated at equilibrium based on the following equation

$$q_e = \frac{(C_0 - C_e)V}{m} \quad (1)$$

where C_0 and C_e (mg/L) were the concentrations of MFX, CIP, and OFLX at initial and equilibrium; m (g) was the mass of adsorbent, and V (L) represented the volume of MFX, CIP, and OFLX solutions.

2.3.1. Adsorption Isotherms and Thermodynamics. As shown in the Supporting Information, 5 mg of adsorbents were added to a series of 20 mL of solutions of MFX, CIP, and OFLX, and batch adsorption experiments were conducted at a definite concentration (0−80 mg/L) and pH of 7.0 ± 0.2. Then, the mixture was shaken at different temperatures (15, 25, 35, and 45 °C) for 12 h at 180 rpm.

2.3.2. Adsorption Kinetics. Adsorption kinetic experiments were carried out with three different concentrations (10, 25, and 50 mg/L) of MFX, CIP, and OFLX. The adsorption capacities for MFX, CIP, and OFLX at a specific time were calculated according to the equation

$$q_t = \frac{(C_0 - C_t)V}{m} \quad (2)$$

where C_t (mg/L) and q_t (mg/g) were the concentrations and removal capacities of MFX, CIP, and OFLX when the time was t (min). The experimental data of adsorption for MFX, CIP,

https://doi.org/10.1021/acsomega.4c07479
ACS Omega 2024, 9, 48618−48628

and OFLX were simulated with three widely used kinetic models: pseudo-first-order (PFO), pseudo-second-order (PSO), and intraparticle diffusion models. The adsorption kinetic curves that conformed to the intraparticle diffusion model are displayed in the Supporting Information. The expressions of these three models are expressed as the following equations

$$q_t = q_e(1 - e^{-k_1 t}) \quad (3)$$

$$q_t = \frac{q_e^2 k_2 t}{1 + k_2 q_e t} \quad (4)$$

$$q_t = k_i t^{0.5} + C \quad (5)$$

where q_e (mg/g) was the adsorption capacity of BC-700 at equilibrium; k_1 (min^{-1}), k_2 (g/mg·min), and k_i (g/mg·$min^{0.5}$) represented the adsorption rate constants of the three kinetic models; C represented the adsorption degree of BC-700 for MFX, CIP, and OFLX.

3. RESULTS AND DISCUSSION

3.1. Characterization of Materials. Bamboo biochar at 400, 500, 600, 700, and 800 °C (BC-400, BC-500, BC-600, BC-700, and BC-800) were analyzed by scanning electron microscopy (SEM), energy dispersive X-ray spectroscopy (EDS), thermogravimetry (TGA), Brunauer−Emmett−Teller (BET) and ζ-potentials. The SEM images and EDS diagrams could be seen in Figures S1 and S2. Figure S1 shows the microstructure of biochar at different pyrolysis temperatures. SEM characterization showed that raw bamboo had a loose sheet structure, while the biochar obtained after pyrolysis had an irregular block structure with a large number of well-developed pores. Before 700 °C, the higher the pyrolysis temperature, the larger the pores, and the surface of BC-700 presented a honeycomb structure. Previous studies had reported that biochar pores were gaps between microcrystals similar to slits or wedges.[19] However, as reported in the research,[26] the bamboo biochar calcined at 800 °C had the appearance of pore collapse, which also explained the decline of the adsorption capacity of bamboo biochar at 800 °C. Higher pyrolysis temperature might lead to the decrease of functional group diversity on the surface of biochar, which in turn affects the adsorption process.[27] As shown in Figure S2, the energy spectrum analysis (EDS) images further compared the differences in element composition and content between raw bamboo and BC-700. The characterization results showed that raw bamboo and BC-700 were mainly composed of carbon and oxygen. After calcination at 700 °C, the relative mass fraction of carbon in bamboo biochar was increased compared with raw bamboo, which might make BC-700 have a good adsorption effect. In Figure 1(a), the N_2 adsorption−desorption isotherms and pore size distribution of BC-700 showed the characteristics of type IV isotherm (H4).[28] Table 1 shows the specific surface area and pore volume of biochar. The higher the pyrolysis temperature, the larger the BET surface area of biochar, and BC-800 had the largest specific surface area, about 586.05 m^2/g. However, BC-700 had the highest pore volume and average pore size, about 0.1538 cm^3/g and 3.3576 nm. The pore size distribution further showed that BC-700 biochar was mainly composed of a micropore structure.

Table 1. Specific Surface Area and Pore Volume of Biochar

samples	BET surface area (m^2/g)	pore volume (cm^3/g)	average pore size (nm)
BC-400	392.12	0.0254	2.5499
BC-500	470.10	0.0556	2.6299
BC-600	493.16	0.1183	3.2748
BC-700	529.31	0.1538	3.3576
BC-800	586.05	0.1374	3.3566

The thermogravimetric curve described the weight loss in the process of carbonization at a temperature of 30−800 °C. Bamboo contained a high content of cellulose, hemicellulose, and lignin,[29] which made it have a larger surface area,[30] movable substances, and carbon content.[31] As shown in Figure 1(b), the weight loss of raw bamboo could be divided into three stages.[32,33] G was the mass fraction, which stood for the y-axis title of the TG curve, and the mass fraction decreased from top to bottom. 30−150 °C was the first stage of biochar weight loss, with the maximum at 70.2 °C. This was caused by evaporation and dehydration, which was the process of water precipitation inside the biomass.[32] The second weight loss was 150−300 °C, which was due to the thermal decomposition of hemicellulose, cellulose, and lignin.[34] The third stage of weight loss occurred between 300 and 800 °C, primarily due to the hydrogen and carbon reduction of lignin.[35] This reduction reaction could remove oxygen-containing functional groups from the lignin structure, leading to a change in weight.[36,37] Further thermal decomposition of intermediate products generated during the reduction reactions also contributed to the weight reduction. The thermogravimetric curve gradually stabilized at 700 °C, indicating that the thermal decomposition reactions had essentially ceased.

As shown in Figure 1(c), the above trend might be related to ζ-potentials and the existing types of MFX, CIP, and OFLX. The distribution coefficients varying with pH are displayed in Figure S3. These indicated that they existed as cations, zwitterions, and anions at different pH values. As shown in Figure 1(d−f), at pH 7.0 ± 0.2, the adsorption capacities of biochar for MFX, CIP, and OFLX increased continuously with the increase of pyrolysis temperature in the range of 400−700 °C, but it increased slowly or decreased slightly at 800 °C.

3.2. Batch Adsorption Experiment. In order to further explore the adsorption performance of MFX, CIP, and OFLX, BC-700 was selected as the representative study.

3.2.1. Adsorption Isotherms and Thermodynamics. With the increase of equilibrium concentration, the adsorption capacities for MFX, CIP, and OFLX increased and then remained stable. In addition, the adsorption capacities of BC-700 increased as the equilibrium concentration rose, and the higher temperature was conducive to the removal of MFX and OFLX, while the lower temperature favored the removal of CIP. Langmuir and Freundlich models were used to simulate the adsorption isotherms for MFX, CIP, and OFLX. The adsorption isotherms of BC-700 for MFX, CIP, and OFLX are shown in Figure 2, and the corresponding parameters are listed in Table 2.

Compared with the Freundlich model, the Langmuir model obtained a relatively high correlation coefficient (R^2), indicating that the removal of MFX, CIP, and OFLX by BC-700 occurred on the homogeneous surface. According to the fitting results of the Langmuir adsorption model, the maximum adsorption capacity of BC-700 for CIP was 151.31 mg/g at 15

https://doi.org/10.1021/acsomega.4c07479
ACS Omega 2024, 9, 48618−48628

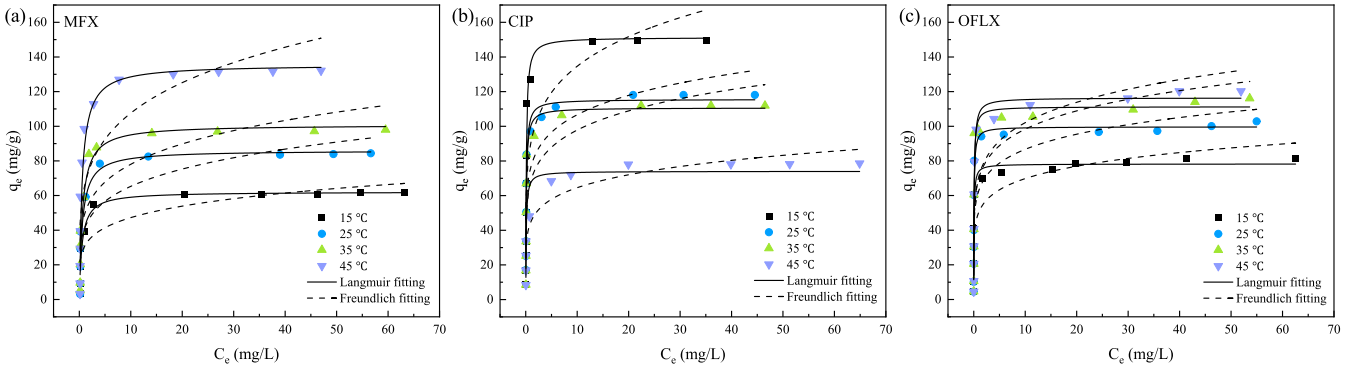

Figure 2. Adsorption isotherms of BC-700 for (a) MFX, (b) CIP, and (c) OFLX conformed to Langmuir and Freundlich models (conditions: adsorbent dosage: 0.25 g/L, concentration of MFX, CIP, and OFLX: 50 mg/L, temperatures: 15, 25, 35, and 45 °C, and pH = 7.0 ± 0.2).

Table 2. Isothermal Parameters of Adsorption for MFX, CIP, and OFLX by BC-700

		Langmuir			Freundlich		
adsorbate	temperature (°C)	K_L (L/mg)	q_{max} (mg/g)	R^2	K_F	N	R^2
MFX	15	1.87	62.17	0.9251	30.5	5.28	0.7828
	25	1.70	86.06	0.9243	40.70	4.87	0.7544
	35	1.63	100.83	0.9431	48.93	4.93	0.7302
	45	1.82	135.56	0.9295	65.04	4.58	0.7514
CIP	15	9.28	151.31	0.9320	90.55	5.80	0.7162
	25	9.69	115.55	0.9503	76.56	6.94	0.7575
	35	9.73	110.66	0.9336	68.53	6.47	0.7433
	45	2.62	77.12	0.9191	43.26	5.96	0.8986
OFLX	15	17.00	78.23	0.9516	50.49	7.12	0.7793
	25	16.12	99.68	0.9090	62.99	7.22	0.6997
	35	14.37	111.29	0.9074	70.08	6.80	0.7010
	45	11.34	116.40	0.9676	71.04	6.35	0.7695

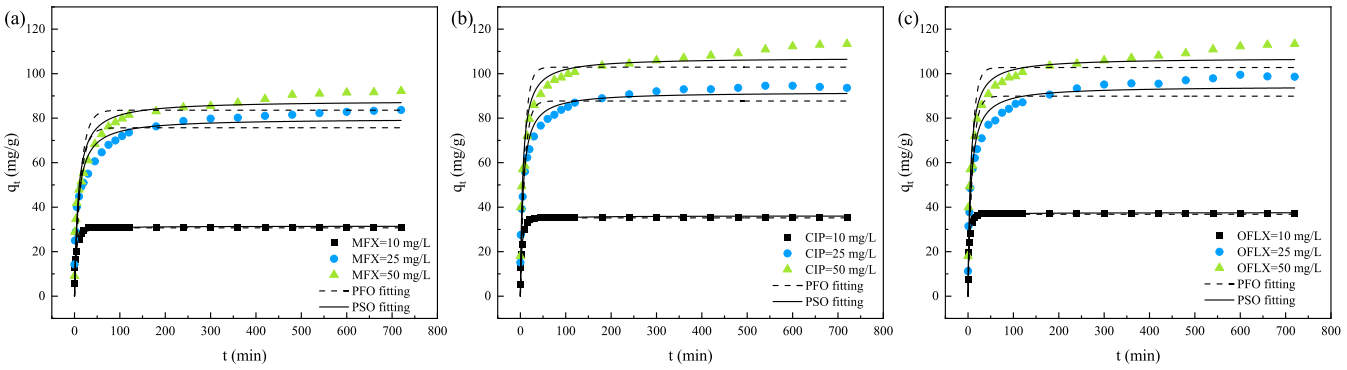

Figure 3. Adsorption kinetic curves of BC-700 for (a) MFX, (b) CIP, and (c) OFLX conformed to PFO and PSO models (conditions: adsorbent dosage: 0.25 g/L, concentrations of MFX, CIP, and OFLX: 10, 25, 50 mg/L, respectively, temperatures: 25 °C, and pH = 7.0 ± 0.2).

Table 3. Kinetic Parameters of Adsorption for MFX, CIP, and OFLX by BC-700

		Pseudo-first-order model			Pseudo-second-order model		
adsorbate	concentration (mg/L)	k_1 (min^{-1})	q_e (mg/g)	r^2	k_2 (min^{-1})	q_e (mg/g)	r^2
MFX	10	0.2461	30.71	0.9157	1.49×10^{-2}	31.48	0.9457
	25	0.0793	75.68	0.7885	158×10^{-3}	79.85	0.9005
	50	0.0745	83.58	0.8172	1.41×10^{-3}	87.93	0.9174
CIP	10	0.2442	35.20	0.9550	1.26×10^{-2}	36.11	0.9646
	25	0.1063	87.72	0.8513	1.89×10^{-3}	91.81	0.9404
	50	0.1094	102.91	0.7989	1.78×10^{-3}	107.22	0.9034
OFLX	10	0.4066	36.80	0.8801	2.15×10^{-2}	37.54	0.9329
	25	0.1027	89.89	0.8254	1.73×10^{-3}	94.38	0.9271
	50	0.1099	102.77	0.7972	1.78×10^{-3}	107.10	0.9024

https://doi.org/10.1021/acsomega.4c07479
ACS Omega 2024, 9, 48618−48628

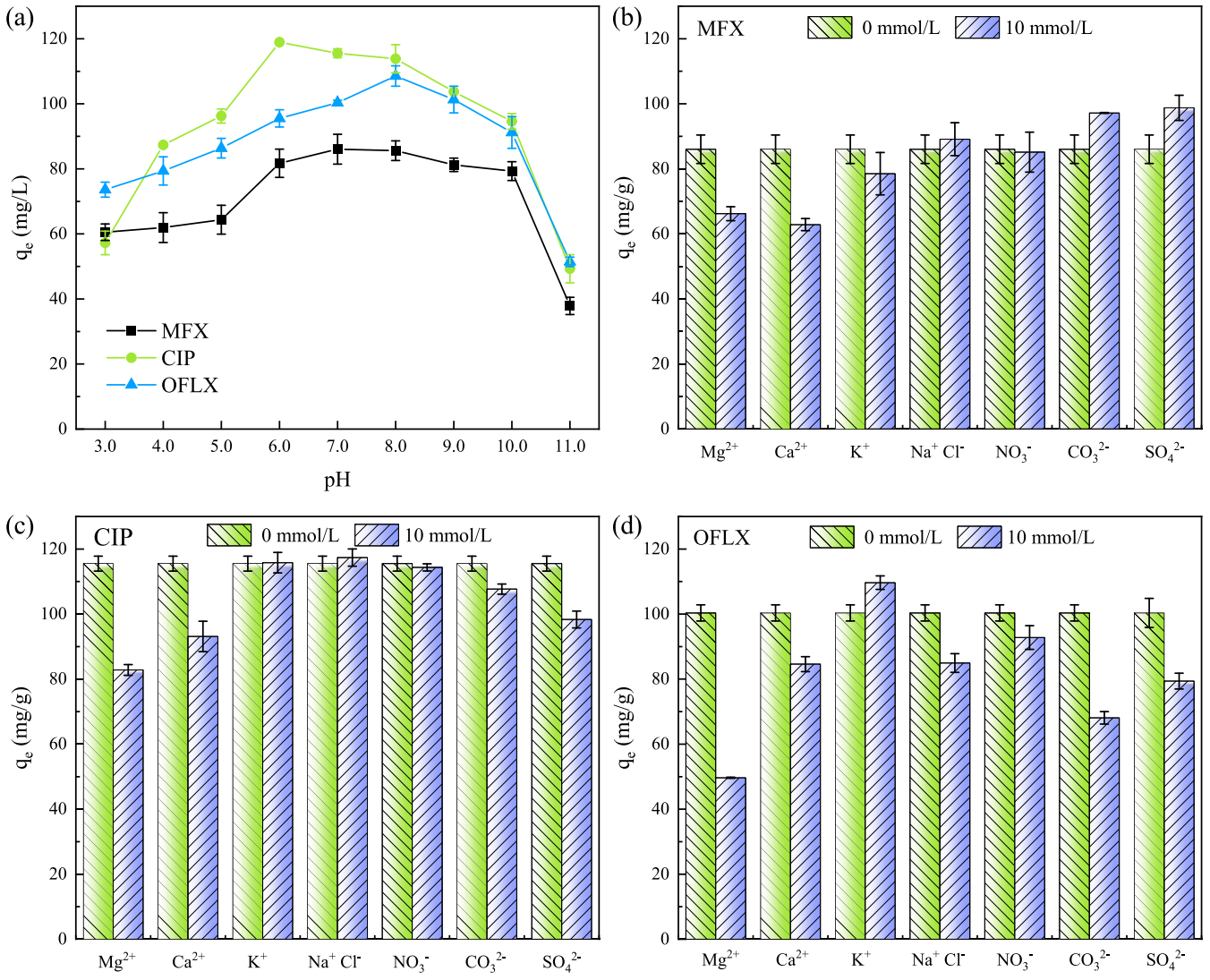

Figure 4. Effect of (a) pH and (b−d) coexisting ions on adsorption of BC-700 for MFX, CIP, and OFLX (conditions: adsorbent dosage: 0.25 g/L, concentration of MFX, CIP, and OFLX: 50 mg/L, temperature: 25 °C, pH 7.0 ± 0.2, rotational speed: 180 rpm).

°C, and the maximum adsorption capacities for MFX and OFLX were 135.56 and 116.40 mg/g at 45 °C, respectively. The results indicated that BC-700 had a relatively high adsorption capacity. Therefore, BC-700 was a promising adsorbent for the treatment of water contaminated with MFX, CIP, and OFLX.

In addition, to further demonstrate the adsorption nature of BC-700 for MFX, CIP, and OFLX, the thermodynamic parameters at each temperature were determined using eqs S(3) and S(4). Thermodynamic parameters for MFX, CIP, and OFLX adsorption onto BC-700 are displayed in the Supporting Information. As illustrated in Table S2, the negative ΔG and positive ΔH values implied spontaneous and endothermic nature, respectively. The positive ΔS value manifested the increased disorder and randomness at the solid−liquid interface during the adsorption for MFX, CIP, and OFLX on the BC-700 surface.[38]

3.2.2. Adsorption Kinetics. Because the appropriate kinetic model provided valuable insights into the rate control steps and potential absorption mechanisms, pseudo-first-order and pseudo-second-order models were applied to simulate BC-700. To improve the applicability and avoid interfering with the experimental results, the pH used in the kinetic study was about 7.0. The adsorption kinetic curves are shown in Figure 3, and the relevant kinetic parameters are listed in Table 3. According to the kinetic curves, it reached saturation in about 3 h, so the following adsorption experiments were carried out with a contact time of 12 h. Comparing the correlation coefficient (R^2), PSO showed a better correlation for all concentrations of MFX, CIP, and OFLX, which described that the rate-limiting step of the adsorption process was chemical adsorption. Therefore, the rate-limiting step of removing MFX, CIP, and OFLX by BC-700 was predicted as chemical adsorption.[39]

The adsorption kinetic curves that conformed to the intraparticle diffusion model are displayed in Figure S4. The adsorption process of BC-700 on MFX, CIP, and OFLX included three steps. The first step was the rapid diffusion of MFX, CIP, and OFLX to the surface of BC-700, and the adsorption rate was the fastest at this stage, which was related to the surface adsorption because there were a large number of adsorption sites or functional groups in BC-700 in the initial adsorption stage.[39] In the second step, MFX, CIP, and OFLX diffused into the pores of BC-700, and the adsorption rate in

https://doi.org/10.1021/acsomega.4c07479
ACS Omega 2024, 9, 48618−48628

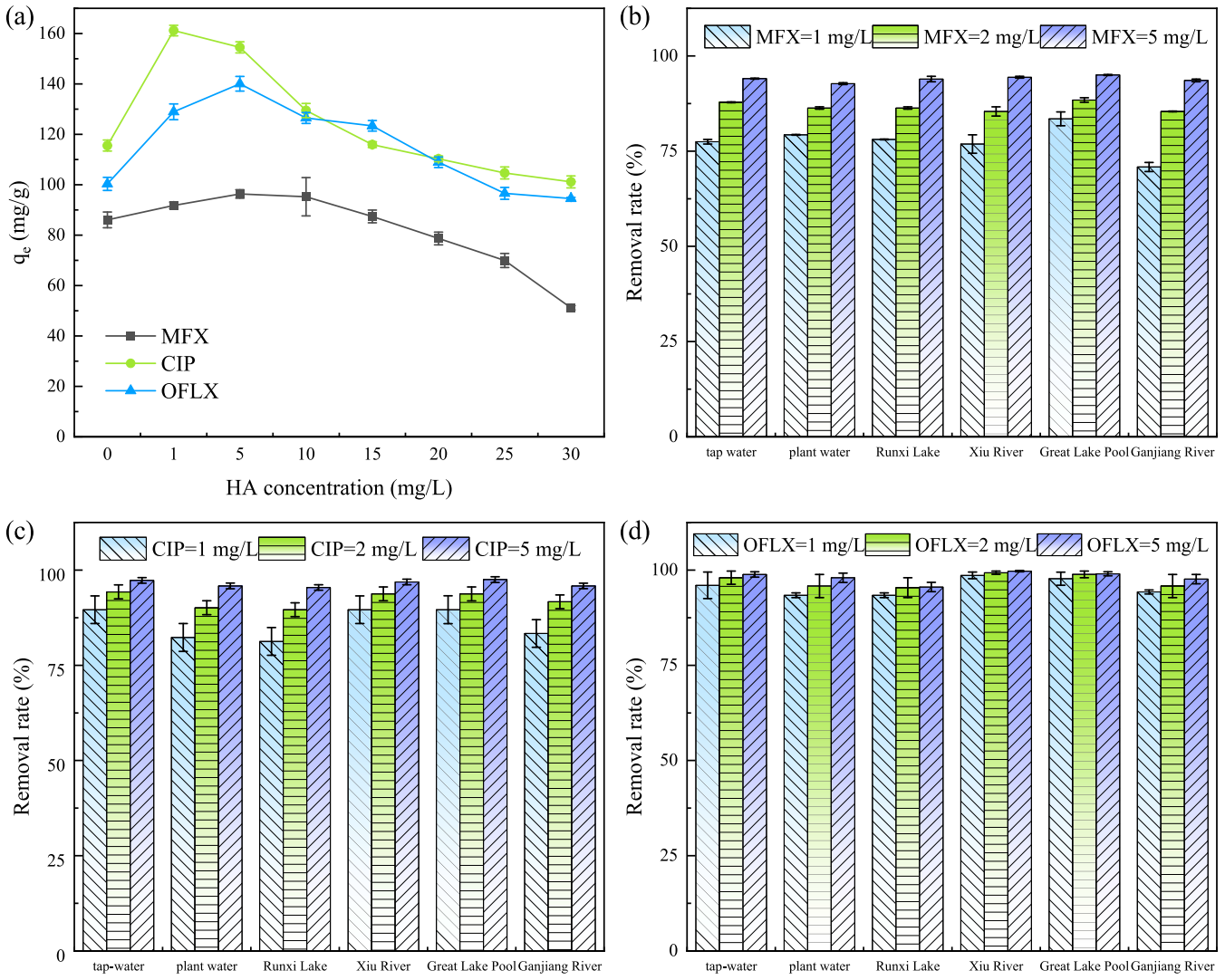

Figure 5. Effect of (a) HA concentration and (b–d) actual water on adsorption of BC-700 for MFX, CIP, and OFLX (conditions: adsorbent dosage: 0.25 g/L, temperature: 25 °C, pH 7.0 ± 0.2, rotational speed: 180 rpm).

the second step was slower than that in the first step, which might be because MFX, CIP, and OFLX occupied the most active sites on the surface of BC-700.[40] The third stage was the adsorption equilibrium process, and the adsorption rate was slow. At this time, the active sites on the BC-700 surface were basically saturated.[41]

3.2.3. Influence of pH. Among the external parameters of the adsorption process, pH was considered to be one of the most important factors. The change of pH could not only alter the surface charge of the adsorbent but also affect the existing form of adsorbates in the solution.[11] So as to further explore the influence of pH on the absorption for MFX, CIP, and OFLX, batch adsorption experiments were carried out at different pH values of the solution, and the corresponding results are shown in Figure 4(a). According to the literature, the pK_a values of MFX, CIP, and OFLX were 6.31 ± 0.50,[42] 5.90 ± 0.15,[43] and 6.10 ± 0.40,[44] respectively.

In Figure 4(a), as the pH increased from 3.0 to 5.0, the adsorption capacity of BC-700 for MFX, CIP, and OFLX increased sharply, then reached a relatively stable level when the pH increased from 6.0 to 8.0 and later decreased to a low value. Discontinuous changes in the adsorption capacity of BC-700 for MFX, CIP, and OFLX showed that different pH regions involved different adsorption mechanisms, so the pH regions were roughly divided into three different blocks. The main reason was that the pH significantly changed the surface charge distribution characteristics of biochar.

As shown in Figure 1(c), when the pH was from pH 3.0 to 5.0, the ζ-potentials of bamboo biochar decreased significantly, and the main existing forms of MFX, CIP, and OFLX were MFX^+, CIP^+, and $OFLX^+$. According to the pK_a of MFX, CIP, and OFLX, they were all positively charged,[45] so it could be determined that electrostatic repulsion had occurred on the surface of biochar. In this pH range, the electrostatic repulsion increased with the increase of pH. Therefore, at low pH (3.0–5.0), the adsorption capacity of bamboo biochar for MFX, CIP, and OFLX increased, which could be attributed to electrostatic interaction. When the pH value was from pH 6.0 to 8.0, ion exchange and cation–π interaction were weakened, and the adsorption capacity of BC-700 showed a relatively high level, which might be caused by hydrogen bonding, π–π interaction, and hydrophobic interaction participating in the adsorption process.[11] At the same time, the positive charge on the surface of biochar was weakened by deprotonation; that was to say, although electrostatic repulsion remained, its force intensity was significantly reduced.[1] When the pH exceeded 8.0, the ζ-

https://doi.org/10.1021/acsomega.4c07479
ACS Omega 2024, 9, 48618–48628

potentials of bamboo biochar changed little, and the decrease of MFX^+, CIP^+, and $OFLX^+$ weakened the electrostatic attraction. In addition, at high pH 9.0−11.0, MFX, CIP, and OFLX mainly existed in the form of negative ions, and the adsorption for MFX, CIP and OFLX by BC-700 also existed $\pi-\pi$ interaction in this range.[1] In addition, with the increase of pH, MFX, CIP, OFLX, and BC-700 were gradually negatively charged, and the electrostatic repulsion at pH 11.0 was enhanced compared with that at pH 9.0. It could be concluded that the adsorption capacity of bamboo biochar would be further reduced. In addition, judging from the structure of bamboo biochar with MFX, CIP, and OFLX, the benzene rings in MFX, CIP, and OFLX could be used as electron acceptors due to the strong electronegativity of the connected fluorine atoms, and the benzene rings introduced on the surface of bamboo biochar could give electrons and serve as π electron donors.[45] Therefore, the electron donor−acceptor interaction might be responsible for the removal of MFX, CIP, and OFLX in the adsorption process. Based on the analysis of the characterization results, electrostatic interaction was also one of the driving forces for the adsorption process.

3.2.4. Influence of Coexisting Ions. The influence of coexisting ions on the adsorption performance of BC-700 was studied at pH 7.0 ± 0.2 in the presence of 10 mmol/L Mg^{2+}, Ca^{2+}, K^+, Na^+, NO_3^+, CO_3^{2+}, and SO_4^{2+} as illustrated in Figure 4(b−d). $MgCl_2$, $CaCl_2$, KCl, NaCl, $NaNO_3$, $NaCO_3$, and $NaSO_4$ were used to add Mg^{2+}, Ca^{2+}, K^+, Na^+, NO_3^+, CO_3^{2+}, and SO_4^{2+} to the solution. The results further confirmed that the possible mechanisms were cation exchange and electrostatic attraction. The concentration of major ions in actual water is displayed in Table S3.

Because the ions existing in natural water, including Mg^{2+}, Ca^{2+}, K^+, Na^+, Cl^-, NO_3^-, CO_3^{2-}, and SO_4^{2-} would affect the adsorption for MFX, CIP, and OFLX, the possibility of competition was verified. It was observed from Figure 4(b−d) that different coexisting ions had different effects on the removal of MFX, CIP, and OFLX.

The influence of lower valence ions on the adsorption of BC-700 for MFX, CIP, and OFLX was basically less than that of higher valence ions, which might be attributed to two aspects. First, higher valence ions were easier to adsorb on the adsorbent surface, so higher valence ions had a greater influence on the adsorption of BC-700 than lower valence ions. Second, a single higher valence ion could reduce two ion interaction sites on the BC-700 surface, while lower valence ions only occupied one site, thus causing this phenomenon.

3.2.5. Influence of Humic Acid. Humic acid (HA) was an organic matter derived from plant residues, which was accumulated by microbial decomposition and transformation and was widely used in agriculture, forestry, animal husbandry, and chemical industry.[46] As a common dissolved organic matter, HA was ubiquitous in the environment and could participate in the interaction of pollutants.[47] Although the existence of HA would pollute groundwater and surface water, its advantages outweighed its disadvantages in treating industrial wastewater, and it could be completely cleaned after advanced treatment. In addition, the surface of HA was rich in functional groups, including carboxyl, hydroxyl, and carbonyl, which made it have a strong affinity for environmental pollutants.[48,49] These groups could exchange ions, adsorb, complex, and chelate with cationic substances. Therefore, it was expected that HA would have a certain impact on BC's removal of pollutants. Dissolved HA was the reason for the adsorption attenuation of biologically activated carbon due to competition for surface adsorption sites and pore blockage.[50,51] In this study, the influence of humic acid (HA) on the removal of MFX, CIP, and OFLX was explored. As shown in Figure 5(a), when the concentration of HA increased from 0 to 3 mg/L, the adsorption capacity of BC-700 for MFX, CIP, and OFLX increased and then decreased. Therefore, when the concentration of HA was low, the existence of HA could promote the removal of MFX, CIP, and OFLX. It could be seen that the low concentration of HA had a strong synergistic effect with BC-700 for MFX, CIP, and OFLX. At pH 7.0, the maximum removal capacities for MFX, CIP, and OFLX were 96.34, 161.19, and 140.07 mg/g, respectively. The possible mechanism was that HA could cause additional complexation, thus enhancing the removal effect of MFX, CIP, and OFLX. HA was rich in oxygen-containing functional groups (carboxyl, phenolic hydroxyl, quinone functional groups, etc.), which could form stable complexes through van der Waals forces, hydrogen bonding, and electrostatic adsorption.[52] It was also possible that HA could closely bond with the surface of BC-700 so that BC-700 could remove cation and anion pollutants more effectively in this process.[53] In the process of adsorbing MFX, CIP, and OFLX, HA bonded on the BC-700 surface could cause additional MFX-HA, CIP-HA, and OFLX-HA, thus enhancing the removal effect of MFX, CIP, and OFLX.[54] Adding HA could effectively promote the dispersion of MFX, CIP, and OFLX and make them more easily absorbed by the pores of the porous media. Cheng and others[55] also found that the existence of organic matter could promote adsorption by enhancing steric hindrance and electric double-layer repulsion. In addition, Kahle and others[56] found that organic matter could form organic−inorganic complexes to promote the adsorption of antibiotics. Therefore, the proper addition of HA could improve the adsorption capacity of BC-700 for MFX, CIP, and OFLX.

However, with the increase of HA concentration, the surface properties of BC-700 might change,[57] and the removal capacities for MFX, CIP, and OFLX would slowly decrease. According to the previous literature, HA could be adsorbed and might occupy the adsorption sites of biochar.[58] The competition between HA and antibiotics might lead to a decrease in the removal rate.

3.2.6. Influence of Actual Water. In this study, the removal effects of MFX, CIP, and OFLX in actual water were explored. The images of the actual water polluted by 1, 2, and 5 mg/L MFX, CIP, and OFLX, respectively, are shown in Figure 5(b−d). The removal rates of MFX, CIP, and OFLX by BC-700 were all above 70% and increased with the increase in concentration. The results indicated that BC-700 had universality toward quinolone antibiotics adsorption and was effective in treating low concentrations of MFX, CIP, and OFLX. In short, BC-700 was an outstanding adsorbent for coping with quinolone antibiotics in actual water.

3.3. Mechanisms. To better understand the adsorption mechanisms, BC-700 before and after adsorbing MFX, CIP, and OFLX were analyzed by SEM, EDS, Fourier-transform infrared (FT-IR), and X-ray photoelectron spectroscopy (XPS). As shown in the SEM images (Figure S5), the morphological structure of BC-700 after adsorbing MFX, CIP, and OFLX changed, pores were filled, and the number of pores decreased. The EDS images of BC-700 before and after adsorbing MFX, CIP, and OFLX are shown in Figure S6. The

https://doi.org/10.1021/acsomega.4c07479
ACS Omega 2024, 9, 48618−48628

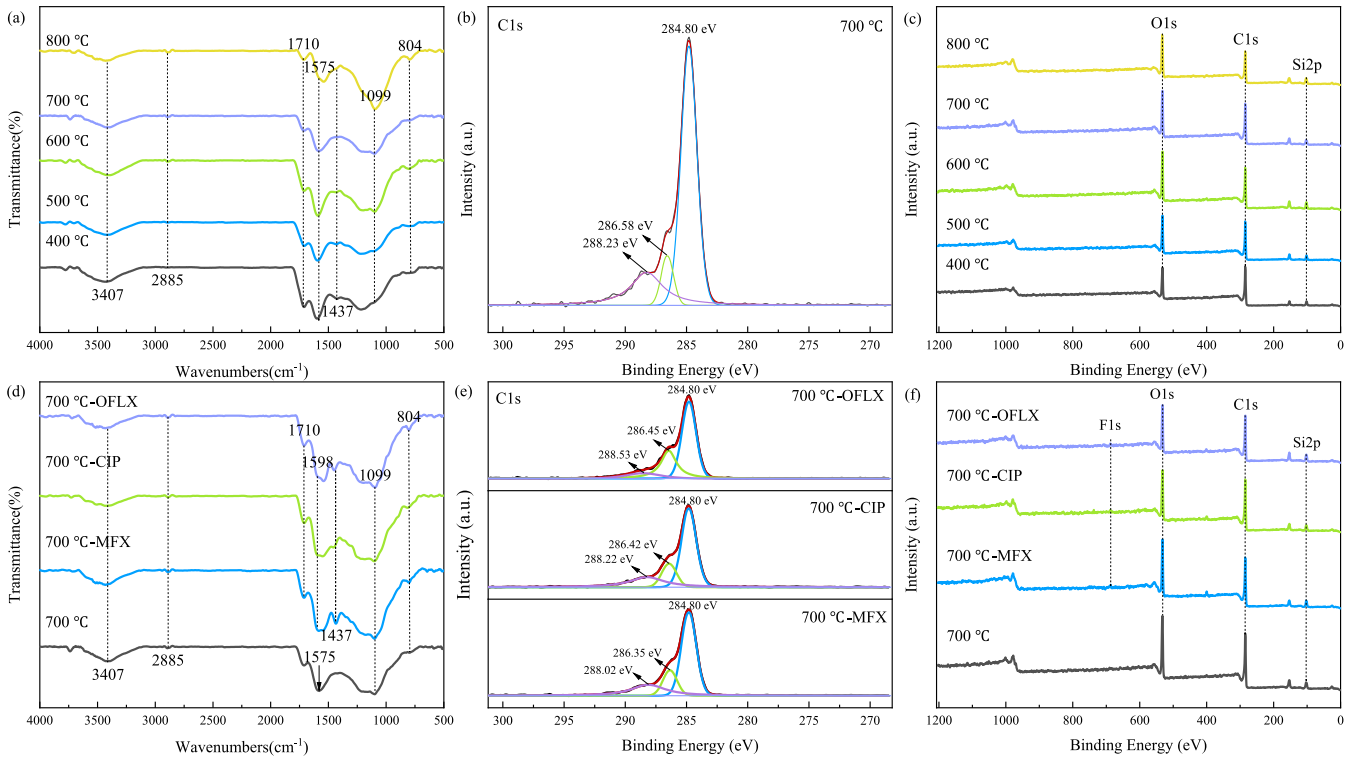

Figure 6. (a, d) FT-IR spectra and (b, c, e, f) XPS curves of BC-700 before and after adsorbing 50 mg/L MFX, CIP, and OFLX.

new F (0.677 keV) peak in the EDS data and all characterization results clearly showed that MFX, CIP, and OFLX were partially adsorbed on the surface of BC-700.

As shown in Figure 6(a,d), there was little difference in the types of functional groups on the surface of bamboo biochar at different pyrolysis temperatures. The broadband around 3407 cm^{-1} was attributed to the stretching of O−H in carboxyl and phenolic hydroxyl groups or the N−H symmetric stretching vibration.[11] The characteristic peak at about 2885 cm^{-1} was due to the existence of the C−H stretch band, which was related to aliphatic functional groups. The peaks around 1710 cm^{-1} corresponded to aromatic C═C or C═O, while the prominent peaks at 1437, 1099, and 804 cm^{-1} were considered to be related to the stretching of C−H_2, aliphatic C−O−C, and aromatic C−H. It was not difficult to see from the FT-IR spectra that the peak intensity of biochar was low at higher pyrolysis temperatures, indicating that the surface functional groups decreased with the increase in pyrolysis temperature.[27]

As shown in Figure 6(b,e), obvious differences were also observed, which confirmed that adsorption could really affect the functional groups of biochar. For the C 1s spectrum of BC-700, the peaks at 284.80, 286.58, and 288.23 eV were related to C−C/C═C, C−O, and C═O, respectively. After adsorbing MFX, CIP, and OFLX, the peak that belonged to C−O transferred to 286.35, 286.42, and 286.45 eV, demonstrating that $\pi-\pi$ interaction might be an important driving force in the adsorption process of BC-700 for MFX, CIP, and OFLX. FT-IR analysis further proved the same adsorption mechanisms, in which the C peak of BC-700 at 1575 cm^{-1} was transferred to 1598 cm^{-1} after absorbing MFX, CIP, and OFLX. These results further verified the hypothesis in 3.2.3.

The high-resolution XPS spectrum of C 1s was obtained. The carbon spectrum of Figure 6(c,f) showed that BC-700 might have a graphite-like structure (284.59 eV in C 1s XPS spectrum), and MFX, CIP, and OFLX molecules had aromatic structures, which might form $\pi-\pi$ stacking interaction. The XPS spectrum of BC-700 before and after absorbing MFX, CIP, and OFLX was studied. A new peak appeared at 687.58 eV, 687.68, and 687.98 eV, which belonged to F in MFX, CIP, and OFLX molecules, indicating the loading of MFX, CIP, and OFLX in BC-700. It was consistent with FT-IR spectrum analysis. MFX, CIP, and OFLX interacted with BC-700 through electrostatic attraction, $\pi-\pi$ stacking of benzene rings, and hydrogen bonding with hydroxyl groups.[2]

3.4. Reusability of BC-700. From a practical point of view, the recyclability and reusability of the spent adsorbents are important characteristics. Based on the analysis of the adsorption mechanisms of BC-700, the adsorbents loaded with MFX, CIP, and OFLX were regenerated by methanol, ethanol, and pyrolysis, respectively, and the adsorption−regeneration cycle was repeated 5 times.

As shown in Table S4, after five cycles, the adsorption capacity of BC-700 in different desorbing agents was compared, and it was determined that methanol was suitable for desorbing MFX, CIP, and OFLX from BC-700. The results further showed that electrostatic interaction was the key driving force for the absorption of BC-700 for MFX, CIP, and OFLX. As shown in Table S5, it was observed that the adsorption performance of BC-700 for MFX, CIP, and OFLX decreased after the first use, which might be due to the difficulty in completely removing MFX, CIP, and OFLX molecules and the incomplete recovery of active sites on the adsorbent. After three adsorption−regeneration cycles, the adsorption capacity of BC-700 for MFX, CIP, and OFLX could still remain above 85%, indicating that BC-700 possessed acceptable reusability.

https://doi.org/10.1021/acsomega.4c07479
ACS Omega 2024, 9, 48618−48628

4. CONCLUSIONS

To remove MFX, CIP, and OFLX, bamboo biochar with different pyrolysis temperatures was synthesized in this study. After comparison, the pyrolysis temperature of 700 °C led to a high pore volume and average pore size of biochar. The biochar produced at 700 °C presented high adsorption properties for MFX, CIP, and OFLX (135.56, 151.31, and 116.40 mg/g), fast adsorption kinetics, wide pH adaptability (3.0−11.0), and the synergistic effect with the low concentration of humic acid. Bamboo biochar could be applied as low-cost adsorbents for quinolone antibiotics removal and had promising applications.

■ ASSOCIATED CONTENT

Supporting Information

The Supporting Information is available free of charge at https://pubs.acs.org/doi/10.1021/acsomega.4c07479.

Additional details of batch experiments, characterization, and reusability, including figures of SEM images, EDS mappings, species distribution at various pH, and intraparticle diffusion model; tables of the partial physicochemical properties of MFX, CIP, and OFLX, thermodynamic parameters, concentrations of major ions in actual water, the results of desorption, and the removal rate after 5 cycles (PDF)

■ AUTHOR INFORMATION

Corresponding Author

Rui Zhao − *School of Resources and Environment and Key Laboratory of Poyang Lake Environment and Resource Utilization, Ministry of Education, Nanchang University, Nanchang, Jiangxi 330031, China;* orcid.org/0009-0005-7558-5212; Email: zr6512@ncu.edu.cn

Authors

Erming Ouyang − *School of Resources and Environment and Key Laboratory of Poyang Lake Environment and Resource Utilization, Ministry of Education, Nanchang University, Nanchang, Jiangxi 330031, China*

Ruiyue Zhang − *Zhejiang Design Institute of Water Conservancy and Hydroelectric Power (ZDWP), Hangzhou, Zhejiang 310002, China; School of Resources and Environment, Nanchang University, Nanchang, Jiangxi 330031, China*

WenJie Fu − *School of Resources and Environment, Nanchang University, Nanchang, Jiangxi 330031, China*

Hongwei Yang − *School of Resources and Environment, Nanchang University, Nanchang, Jiangxi 330031, China*

Hanrui Xiang − *School of Resources and Environment, Nanchang University, Nanchang, Jiangxi 330031, China*

Wanyuan He − *School of Resources and Environment, Nanchang University, Nanchang, Jiangxi 330031, China*

Complete contact information is available at: https://pubs.acs.org/10.1021/acsomega.4c07479

Notes

The authors declare no competing financial interest.

■ ACKNOWLEDGMENTS

Financial support from the Natural Science Foundation of Jiangxi Province (20232BAB214088) is gratefully acknowledged.

■ REFERENCES

(1) Gao, B.; Li, P.; Yang, R.; Li, A.; Yang, H. Investigation of multiple adsorption mechanisms for efficient removal of ofloxacin from water using ligninbased adsorbents. *Sci. Rep.* **2019**, *9* (1), No. 637, DOI: 10.1038/s41598-018-37206-1.

(2) Zheng, C.; Zheng, H.; Hu, C.; Wang, Y.; Wang, Y.; Zhao, C.; Ding, W.; Sun, Q. Structural design of magnetic biosorbents for the removal of ciprofloxacin from water. *Bioresour. Technol.* **2020**, *296*, No. 122288, DOI: 10.1016/j.biortech.2019.122288.

(3) Zheng, C.; Zheng, H.; Wang, Y.; Sun, Y.; An, Y.; Liu, H.; Liu, S. Modified magnetic chitosan microparticles as novel superior adsorbents with huge "force field" for capturing food dyes. *J. Hazard. Mater.* **2019**, *367*, 492−503, DOI: 10.1016/j.jhazmat.2018.12.120.

(4) Lu, Z.; Deng, F.; He, R.; Tan, L.; Luo, X.; Pan, X.; Yang, Z. A pass-through solid-phase extraction clean-up method for the determination of 11 quinolone antibiotics in chicken meat and egg samples using ultra-performance liquid chromatography tandem mass spectrometry. *Microchem. J.* **2019**, *151*, No. 104213, DOI: 10.1016/j.microc.2019.104213.

(5) Zhao, R.; Ding, W.; Sun, M.; Yang, L.; Liu, B.; Zheng, H.; Li, H. Insight into the co-removal of Cu(II) and ciprofloxacin by calcite-biochar composite: Enhancement and competition. *Sep. Purif. Technol.* **2022**, *287*, No. 120487, DOI: 10.1016/j.seppur.2022.120487.

(6) Deng, J.; Li, X.; Wei, X.; Liu, Y.; Liang, J.; Song, B.; Shao, Y.; Huang, W. Hybrid silicate-hydrochar composite for highly efficient removal of heavy metal and antibiotics: Coadsorption and mechanism. *Chem. Eng. J.* **2020**, *387*, No. 124097, DOI: 10.1016/j.cej.2020.124097.

(7) Hu, C.; Jiang, J.; An, Y.; Jiang, X.; Sun, Q.; Zheng, H.; Li, H. A novel self-floating silica adsorbent for antibiotic ciprofloxacin and nickel (II) ion. *Chem. Eng. J.* **2022**, *429*, No. 132227, DOI: 10.1016/j.cej.2021.132227.

(8) Zheng, Y.; Zhuang, W.; Zhao, M.; Zhang, J.; Song, Y.; Liu, S.; Zheng, H.; Zhao, C. Role of driven approach on the piezoelectric ozonation processes: Comparing ultrasound with hydro-energy as driving forces. *J. Hazard. Mater.* **2021**, *418*, No. 126392, DOI: 10.1016/j.jhazmat.2021.126392.

(9) Zhang, Y.; Chen, J.; Hua, L.; Li, S.; Zhang, X.; Sheng, W.; Cao, S. High photocatalytic activity of hierarchical SiO2@C-doped TiO2 hollow spheres in UV and visible light towards degradation of rhodamine B. *J. Hazard. Mater.* **2017**, *340*, 309−318, DOI: 10.1016/j.jhazmat.2017.07.018.

(10) Jing, L.; Xuejiang, W.; Yuan, W.; Siqing, X.; Jianfu, Z. Insight into the co-adsorption behaviors and interface interactions mechanism of chlortetracycline and lead onto struvite loaded diatomite. *J. Hazard. Mater.* **2020**, *405*, No. 124210, DOI: 10.1016/j.jhazmat.2020.124210.

(11) Zhao, R.; Zheng, H.; Zhong, Z.; Zhao, C.; Sun, Y.; Huang, Y.; Zheng, X. Efficient removal of diclofenac from surface water by the functionalized multilayer magnetic adsorbent: Kinetics and mechanism. *Sci. Total Environ.* **2021**, *760*, No. 144307, DOI: 10.1016/j.scitotenv.2020.144307.

(12) Li, R.; Zhang, Y.; Deng, H.; Zhang, Z.; Wang, J. J.; Shaheen, S. M.; Xiao, R.; Rinklebe, J.; Xi, B.; He, X.; Du, J. Removing tetracycline and Hg(II) with ball-milled magnetic nanobiochar and its potential on polluted irrigation water reclamation. *J. Hazard. Mater.* **2020**, *384*, No. 121095, DOI: 10.1016/j.jhazmat.2019.121095.

(13) Sun, K.; Dong, S.; Sun, Y.; Gao, B.; Du, W.; Xu, H.; Wu, J. Graphene oxide-facilitated transport of levofloxacin and ciprofloxacin in saturated and unsaturated porous media. *J. Hazard. Mater.* **2018**, *348*, 92−99, DOI: 10.1016/j.jhazmat.2018.01.032.

(14) Pan, J.; Gao, B.; Song, W.; Xu, X.; Yue, Q. Modified biogas residues as an eco-friendly and easily-recoverable biosorbent for nitrate and phosphate removals from surface water. *J. Hazard. Mater.* **2020**, *382*, No. 121073, DOI: 10.1016/j.jhazmat.2019.121073.

(15) Zhao, Y.; Li, W.; Liu, J.; Huang, K.; Wu, C.; Shao, H.; Chen, H.; Liu, X. Modification of garlic peel by nitric acid and its application as a novel adsorbent for solid-phase extraction of quinolone

antibiotics. *Chem. Eng. J.* **2017**, *326*, 745−755, DOI: 10.1016/j.cej.2017.05.139.
(16) Wang, L.; Li, Y.; Xu, L.; Sun, D.; Wang, Y.; Wang, Z. Rice straw pretreatment using cow breeding wastewater for methane production. *Bioresour. Technol.* **2021**, *346*, No. 126657, DOI: 10.1016/j.biortech.2021.126657.
(17) Tan, J.; Huang, J.; Yuan, J.; Chen, J.; Pei, Z.; Li, H.; Yang, S. Novel supramolecular deep eutectic solvent-enabled in-situ lignin protection for full valorization of all components of wheat straw. *Bioresour. Technol.* **2023**, *388*, No. 129722, DOI: 10.1016/j.biortech.2023.129722.
(18) Chioma, A. O.; Olubunmi, O. A.; Samson, O. O.; Gloria, T. A.; Abiodun, E. A.; Clement, O. F. Potential application and regeneration of bamboo biochar for wastewater treatment: A review. *Adv. Bamboo Sci.* **2023**, *2*, No. 100012, DOI: 10.1016/j.bamboo.2022.100012.
(19) Wang, B.; Dai, X.; Ma, Y.; Xin, J.; Pan, C.; Zhai, Y. Nitrogen-rich porous biochar for highly efficient adsorption of perchlorate: Influencing factors and mechanism. *J. Environ. Chem. Eng.* **2023**, *11* (3), No. 110293, DOI: 10.1016/j.jece.2023.110293.
(20) Karimipour-Fard, P.; Chio, C.; Brunone, A.; Marway, H.; Thompson, M.; Abdehagh, N.; Qin, W.; ChunzhongYang, T. Lignocellulosic biomass pretreatment: Industrial oriented high-solid twin-screw extrusion method to improve biogas production from forestry biomass resources. *Bioresour. Technol.* **2024**, *393*, No. 130000.
(21) Tomczyk, A.; Sokołowska, Z.; Boguta, P. Biochar physicochemical properties: pyrolysis temperature and feedstock kind effects. *Rev. Environ. Sci. Bio/Technol.* **2020**, *19* (1), 191−215, DOI: 10.1007/s11157-020-09523-3.
(22) Xiang, Y.; Yang, X.; Xu, Z.; Hu, W.; Zhou, Y.; Wan, Z.; Yang, Y.; Wei, Y.; Yang, J.; Tsang, D. C. W. Fabrication of sustainable manganese ferrite modified biochar from vinasse for enhanced adsorption of fluoroquinolone antibiotics: Effects and mechanisms. *Sci. Total Environ.* **2020**, *709*, No. 136079, DOI: 10.1016/j.scitotenv.2019.136079.
(23) Jang, H. M.; Kan, E. Engineered biochar from agricultural waste for removal of tetracycline in water. *Bioresour. Technol.* **2019**, *284*, 437−447, DOI: 10.1016/j.biortech.2019.03.131.
(24) Pan, J.; Gao, B.; Duan, P.; Guo, K.; Xu, X.; Yue, Q. Recycling exhausted magnetic biochar with adsorbed Cu2+ as a cost-effective permonosulfate activator for norfloxacin degradation: Cu contribution and mechanism. *J. Hazard. Mater.* **2021**, *413*, No. 125413, DOI: 10.1016/j.jhazmat.2021.125413.
(25) Sun, K.; Huang, Q.; Chi, Y.; Yan, J. Effect of ZnCl 2 -activated biochar on catalytic pyrolysis of mixed waste plastics for producing aromatic-enriched oil. *Waste Manage.* **2018**, *81*, 128−137, DOI: 10.1016/j.wasman.2018.09.054.
(26) Wang, C.; Wang, Y.; Herath, H. M. S. K. Polycyclic aromatic hydrocarbons (PAHs) in biochar − Their formation, occurrence and analysis: A review. *Org. Geochem.* **2017**, *114*, 1−11.
(27) Pap, S.; Kirk, C.; Bremner, B.; Sekulic, M. T.; Shearer, L.; Gibb, S. W.; Taggart, M. A. Low-cost chitosan-calcite adsorbent development for potential phosphate removal and recovery from wastewater effluent. *Water Res.* **2020**, *173*, No. 115573, DOI: 10.1016/j.watres.2020.115573.
(28) Wang, Y.; Liu, L.; Cheng, H. Gas Adsorption Characterization of Pore Structure of Organic-rich Shale: Insights into Contribution of Organic Matter to Shale Pore Network. *Nat. Resour. Res.* **2021**, *30* (3), 2377−2395, DOI: 10.1007/s11053-021-09817-5.
(29) Gao, B.; Li, P.; Yang, R.; Li, A.; Yang, H. Investigation of multiple adsorption mechanisms for efficient removal of ofloxacin from water using ligninbased adsorbents. *Sci. Rep.* **2019**, *9* (1), No. 637.
(30) Karimipour-Fard, P.; Chio, C.; Brunone, A.; Marway, H.; Thompson, M.; Abdehagh, N.; Qin, W.; Yang, T. C. Lignocellulosic biomass pretreatment: Industrial oriented high-solid twin-screw extrusion method to improve biogas production from forestry biomass resources. *Bioresour. Technol.* **2023**, *393*, No. 130000.
(31) Tomczyk, A.; Sokołowska, Z.; Boguta, P. Biochar physicochemical properties: pyrolysis temperature and feedstock kind effects. *Rev. Environ. Sci. Bio/Technol.* **2020**, *19* (1), 191−215.
(32) Zhao, C.; Shang, D.; Zou, Y.; Du, Y.; Wang, Q.; Xu, F.; Ren, L.; Kong, Q. Changes in electricity production and microbial community evolution in constructed wetland-microbial fuel cell exposed to wastewater containing Pb(II). *Sci. Total Environ.* **2020**, *732*, No. 139127, DOI: 10.1016/j.scitotenv.2020.139127.
(33) Gurten, I. I.; Ozmak, M.; Yagmur, E.; Aktas, Z. Preparation and characterisation of activated carbon from waste tea using K 2 CO 3. *Biomass Bioenergy* **2012**, *37*, 73−81.
(34) Gurten, I. I.; Ozmak, M.; Yagmur, E.; Aktas, Z. Preparation and characterisation of activated carbon from waste tea using K 2 CO 3. *Biomass Bioenergy* **2012**, *37*, 73−81, DOI: 10.1016/j.biombioe.2011.12.030.
(35) Wei, R.; Li, H.; Lin, Y.; Yang, L.; Long, H.; Xu, C.; Li, J. Reduction characteristics of iron oxide by the hemicellulose, cellulose, and lignin components of biomass. *Energy Fuels* **2020**, *34* (7), 8332−8339.
(36) Fu, K.; Yue, Q.; Gao, B.; Sun, Y.; Zhu, L. Preparation, characterization and application of lignin-based activated carbon from black liquor lignin by steam activation. *Chem. Eng. J.* **2013**, *228*, 1074−1082, DOI: 10.1016/j.cej.2013.05.028.
(37) Wang, A. Y.; Sun, K.; Wu, L.; Wu, P.; Zeng, W.; Tian, Z.; Huang, Q. X. Co-carbonization of biomass and oily sludge to prepare sulfamethoxazole super-adsorbent materials. *Sci. Total Environ.* **2020**, *698*, No. 134238, DOI: 10.1016/j.scitotenv.2019.134238.
(38) Song, W.; Gao, B.; Xu, X.; Xing, L.; Han, S.; Duan, P.; Song, W.; Jia, R. Adsorption−desorption behavior of magnetic amine/Fe 3 O 4 functionalized biopolymer resin towards anionic dyes from wastewater. *Bioresour. Technol.* **2016**, *210*, 123−130.
(39) Zheng, X.; Zheng, H.; Zhao, R.; Sun, Y.; Sun, Q.; Zhang, S.; Liu, Y. Polymer-Functionalized Magnetic Nanoparticles: Synthesis, Characterization, and Methylene Blue Adsorption. *Materials* **2018**, *11* (8), 1312.
(40) Zheng, X.; Zheng, H.; Zhao, R.; Xiong, Z.; Wang, Y.; Sun, Y.; Ding, W. Sulfonic acid-modified polyacrylamide magnetic composite with wide pH applicability for efficient removal of cationic dyes. *J. Mol. Liq.* **2020**, *319*, No. 114161, DOI: 10.1016/j.molliq.2020.114161.
(41) Zheng, X.; Zheng, H.; Xiong, Z.; Zhao, R.; Liu, Y.; Zhao, C.; Zheng, C. Novel anionic polyacrylamide-modify-chitosan magnetic composite nanoparticles with excellent adsorption capacity for cationic dyes and pH-independent adsorption capability for metal ions. *Chem. Eng. J.* **2020**, *392*, No. 123706.
(42) Rusu, A.; Tóth, G.; Szőcs, L.; Kökösi, J.; Kraszni, M.; Gyéresi, Á.; Noszál, B. Triprotic site-specific acid−base equilibria and related properties of fluoroquinolone antibacterials. *J. Pharm. Biomed. Anal.* **2012**, *66*, 50−57, DOI: 10.1016/j.jpba.2012.02.024.
(43) Wang, B.; Xu, X.; Tang, H.; Mao, Y.; Chen, H.; Ji, F. Highly efficient adsorption of three antibiotics from aqueous solutions using glucose-based mesoporous carbon. *Appl. Surf. Sci.* **2020**, *528*, No. 147048, DOI: 10.1016/j.apsusc.2020.147048.
(44) Yang, C.; Miao, S.; Li, T. Influence of water washing treatment on Ulva prolifera-derived biochar properties and sorption characteristics of ofloxacin. *Sci. Rep.* **2021**, *11* (1), No. 1797, DOI: 10.1038/s41598-021-81314-4.
(45) Wallis, S. C.; Gahan, L.; Charles, B.; Hambley, T.; Duckworth, P. Copper(II) complexes of the fluoroquinolone antimicrobial ciprofloxacin. Synthesis, X-ray structural characterization, and potentiometric study. *J. Inorg. Biochem.* **1996**, *62*, 1−16.
(46) Pignatello, J. J. Dynamic interactions of natural organic matter and organic compounds. *J. Soils Sediments* **2012**, *12* (8), 1241−1256.
(47) Wang, Y.; Wang, L.; Fang, G.; Herath, H. M. S. K.; Wang, Y.; Cang, L.; Xie, Z.; Zhou, D. Enhanced PCBs sorption on biochars as affected by environmental factors: Humic acid and metal cations. *Environ. Pollut.* **2013**, *172*, 86−93.
(48) Klavins, M.; Purmalis, O. Humic substances as surfactants. *Environ. Chem. Lett.* **2010**, *8* (4), 349−354.

https://doi.org/10.1021/acsomega.4c07479
ACS Omega 2024, 9, 48618−48628

(49) Pignatello, J. J.; Seokjoon, K.; Yufeung, L. Effect of natural organic substances on the surface and adsorptive properties of environmental black carbon (char): attenuation of surface activity by humic and fulvic acids. *Environ. Sci. Technol.* **2006**, *40* (24), 7757−7763.
(50) Koelmans, A. A.; Meulman, B.; Meijer, T.; Jonker, M. T. O. Attenuation of polychlorinated biphenyl sorption to charcoal by humic acids. *Environ. Sci. Technol.* **2009**, *43* (3), 736−742.
(51) Quinlivan, P. A.; Li, L.; Knappe, D. R. U. Effects of activated carbon characteristics on the simultaneous adsorption of aqueous organic micropollutants and natural organic matter. *Water Res.* **2005**, *39* (8), 1663−1673.
(52) Yang, T.; Hodson, M. E. Investigating the use of synthetic humic-like acid as a soil washing treatment for metal contaminated soil. *Sci. Total Environ.* **2019**, *647*, 290−300.
(53) Zhang, Y.; Yin, M.; Sun, X.; Zhao, J. Implication for adsorption and degradation of dyes by humic acid: Light driven of environmentally persistent free radicals to activate reactive oxygen species. *Bioresour. Technol.* **2020**, *307*, No. 123183.
(54) Arslan, G.; Pehlivan, E. Uptake of Cr 3+ from aqueous solution by lignite-based humic acids. *Bioresour. Technol.* **2008**, *99* (16), 7597−7605.
(55) Cheng, T.; Saiers, J. E. Effects of dissolved organic matter on the co-transport of mineral colloids and sorptive contaminants. *J. Contam. Hydrol.* **2015**, *177*−*178*, 148−157.
(56) Kahle, M.; Stamm, C. Time and pH-dependent sorption of the veterinary antimicrobial sulfathiazole to clay minerals and ferrihydrite. *Chemosphere* **2007**, *68* (7), 1224−1231.
(57) Yan, W. L.; Bai, R. Adsorption of lead and humic acid on chitosan hydrogel beads. *Water Res.* **2005**, *39*, 688−698.
(58) Luo, K.; Pang, Y.; Yang, Q.; Wang, D.; Li, X.; Wang, L.; Lei, M.; Liu, J. Enhanced ciprofloxacin removal by sludge-derived biochar: Effect of humic acid. *Chemosphere* **2019**, *231*, 495−501, DOI: 10.1016/j.chemosphere.2019.05.151.

https://doi.org/10.1021/acsomega.4c07479
ACS Omega 2024, 9, 48618−48628